Engineering Structures 242 (2021) 112536

Contents lists available at ScienceDirect

Engineering Structures

journal homepage: www.elsevier.com/locate/engstruct

A variable order framework for 3D nonlinear analysis of reinforced concrete frames under general loading

Mauro Poliotti [a], Jesús-Miguel Bairán [a,*], Oscar Möller [b]

[a] Department of Civil and Environmental Engineering, Universitat Politècnica de Catalunya, (UPC), Jordi Girona, 1-3, Campus Nord, Mod. C-1, 08034 Barcelona, Spain
[b] Instituto de Mecánica Aplicada y Estructuras (IMAE), Universidad Nacional de Rosario, (UNR), Riobamba y Berutti, 2000 Rosario, Argentina

ARTICLE INFO

Keywords:
Reinforced concrete frames
Force-based element
Sectional Interaction
B-splines
Plastic-damage model
OpenSees

ABSTRACT

A framework for the analysis of three-dimensional reinforced concrete frame structures, capable of reproducing general failure modes, is presented. A force-based model which guarantees the equilibrium between nodal and sectional forces is enhanced by means of a cross-sectional model. It is capable of capturing the complex coupling between all the internal forces. Consequently, different failure modes can be reproduced such as shear, torsional, flexural or axial failures. Material modeling of concrete is made using a plastic-damage model that incorporates a variable dilatancy parameter. The sectional and constitutive models are implemented in *OpenSees*. The sectional model can be used at each integration point of the force-based element. Alternatively, it can be used only where high coupling between the internal forces is expected, producing a variable order structural model. The validation shows that the frame element is capable of accurately reproduce beams and columns under monotonic and cyclic loads. The framework presented is a powerful numerical instrument for the analysis, design and assessment of reinforced concrete buildings and bridges.

1. Introduction

Modern guidelines for seismic design or assessment of reinforced concrete buildings and bridges [1–4] require nonlinear static push-over or dynamic analysis of those structures. In that sense, three dimensional finite element (FE) model is a powerful tool. However, the high computational cost of such models makes them prohibitive for the analysis of full scale structures in most practical cases. Hence, practitioners use one dimensional elements when analyzing reinforced concrete structures mainly composed by beams, girders or columns. Frame elements are computationally cheaper and robust. In addition, they are easy to pre- and post- process, and they are directly related to the engineers reasoning.

Classic fiber-beam models [5–9] consist on mixed or force-based frame formulations where, on each integration point the cross-section is discretized into fibers. The fibers are represented by their area and by uniaxial nonlinear constitutive laws for concrete or steel. Fiber-beam models are capable of tracing coupling between axial load and bending moments in a robust manner. Consequently, these models are able to capture axial or flexural failures accurately in many practical cases.

However, most fiber-beam models neglect the coupling between axial and tangential forces, such as shear or torsion [10–12]. As a result, they are not able to reproduce shear or torsional failures. Moreover, as the presence of high shear forces affects the bending response of reinforced concrete elements [12], they loose accuracy on the prediction of flexural failure. Another shortcoming of these models, is that they only consider transverse reinforcements at the material level by means of reinforcement ratios that affect the uniaxial constitutive law of concrete. In order to reproduce confinement, different material properties are defined within the same cross-section and the constitutive laws are recalibrated for different confining materials and arrangements of transverse reinforcements. Consequently, a lost of accuracy and objectivity of fiber-beam models on the reproduction of axial load failure is produced.

Some frame models exist that take into account the shear failure of reinforced concrete elements with different degrees of accuracy and robustness. Detailed state of the art reviews were made by [11,12]. More recent models were developed with aims to incorporate to fiber-beam models different failures modes such as shear or torsion in a coupled way [13–21]. In most cases, this is made by enhancing the beam kinematics altogether with the use of 2D or 3D constitutive models for concrete.

In this paper, a framework capable of tracing the response of reinforced concrete elements under general coupled loading is presented.

* Corresponding author.
E-mail addresses: mauro.poliotti@upc.edu (M. Poliotti), jesus.miguel.bairan@upc.edu (J.-M. Bairán), moller@fceia.unr.edu.ar (O. Möller).

https://doi.org/10.1016/j.engstruct.2021.112536
Received 17 March 2020; Received in revised form 11 April 2021; Accepted 12 May 2021
Available online 5 June 2021

Nomenclature

$\boldsymbol{Q}$	global force vector
$\boldsymbol{D}$	global displacement vector
$\boldsymbol{K}$	structural stiffness matrix
$\boldsymbol{q}$	element nodal force vector
$\boldsymbol{d}$	element nodal displacement vector
$\boldsymbol{K_e}$	element stiffness matrix
$\boldsymbol{\sigma}$	stress tensor
$\boldsymbol{\varepsilon}$	strain tensor
$\boldsymbol{C}$	Material tangent matrix
$\boldsymbol{s_s}$	sectional force vector
$\boldsymbol{e_s}$	sectional generalized deformation vector
$\boldsymbol{k_s}$	sectional stifness matrix according to [25]
N	axial force
V_y, V_z	shear force along y and z axis
T	torsion moment
M_y, M_z	bending moment around y and z axis
ε_0	section generalized axial strain
γ_{0y}, γ_{0z}	section generalized shear deformations along y and z axis
ϕ_x	curvature around x axis, torsion twist per unit length
ϕ_y, ϕ_z	bending curvature around y and z axis
$\boldsymbol{b}$	element force interpolation matrix
$\boldsymbol{f_s}$	sectional flexibility matrix
$\boldsymbol{F_e}$	element flexibility matrix
$\boldsymbol{u}$	section displacement field
$\boldsymbol{u_{ps}}$	section displacement field according to plane section hypothesis
$\boldsymbol{u_w}$	complementary displacement field
$\boldsymbol{N_w}$	sectional interpolation shape function matrix
$\boldsymbol{d_w}$	complementary warping-distortion degrees-of-freedom vector
$\bar{\boldsymbol{\sigma}}$	effective stress tensor
$\boldsymbol{E}_0$	undamaged elastic stifness tensor
$\boldsymbol{\varepsilon}^p$	plastic strain tensor
D	scalar stifness degradation variable according to [32]
$\boldsymbol{\kappa}$	plastic-damage variable vector
$\dot{\lambda}$	plastic consistency parameter
Φ	plastic potential function
$\boldsymbol{H}$	plastic-damage evolution vector according to [32]
F	yield function
α, β, γ	coefficients of yield function according to [32]
I_1	first invariant of stress tensor
J_2	second invariant of deviatoric stress tensor
$\widehat{\bar{\sigma}}$	algebraically maximum principal stress
c_c	compressive cohesion according to [32]
ε_1	eccentricity parameter of the hyperbolic Drucker-Prager function
α_p	dilatancy parameter according to [26]
$\aleph$	auxiliary variable equal to t for tension and c for compression
g_t,g_c	tensile and compressive specific fracture energy parameters
G_t,G_c	fracture and crushing energies
l_{ch}	characteristic length
f_{t0},f_{c0}	initial yield stress for uniaxial tension and compression
$a_\aleph$,$b_\aleph$	parameters for uniaxial strength function according to [32]
ψ^{max},ϕ^{max}	maximum dilatancy and internal friction angles according to [26]

The model involves three different levels: the element level, the cross-section level and the material point. At the frame level, the beam-column formulation introduced in [7,9,22–24] is used as framework. Then, each integration point of the frame element is simulated by means of the total interaction cross-sectional model introduced in [25]. Further, each material point of the concrete cross-section is represented by a 3D plastic-damage model with evolutive dilatancy presented by [26]. The three models are completely independent and its integration for the analysis of frame structures constitutes the main novelty of this work. The joint use of these three independent models constitutes a new tool for nonlinear analysis of frame structure. The model is validated against experimental data available in literature. First, two reinforced

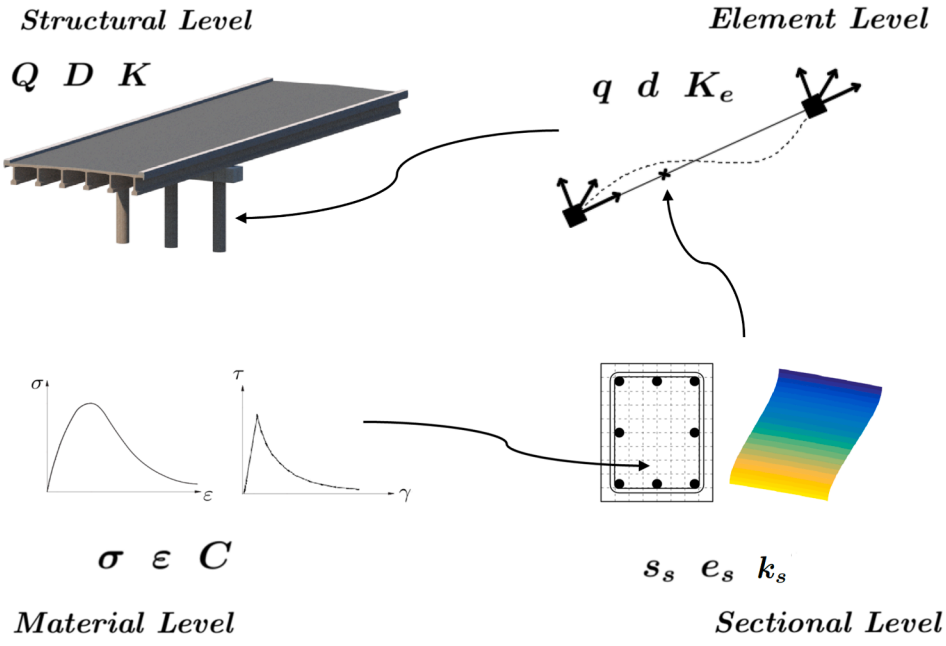

Fig. 1. Proposed Framework.

concrete beams under combined bending and shear are numerically reproduced. Then, a cyclically loaded reinforced concrete column is tested. Finally, in order to demonstrate the capability of the framework for seismic assessment in shear-sensible structures, the performance of a bridge under seismic loads is studied.

2. Proposed framework

The structural analysis of a bridge or building can be divided into four levels, as it is shown in Fig. 1. The structural level involves the determination of global forces $\boldsymbol{Q}$, global displacements $\boldsymbol{D}$ and the structural stiffness matrix that relates them $\boldsymbol{K}$. These variables are obtained by a proper assembly of nodal forces $\boldsymbol{q}$, nodal displacements $\boldsymbol{d}$ and element stiffness $\boldsymbol{K_e}$, respectively (see Fig. 1).

Each column, beam or girder, in most cases, can be represented by a frame element with two nodes. In a general 3D structure, the degrees of freedom on each node are three displacements and three rotations. The corresponding forces of the element are three forces and three moments on each node. At the element level, equilibrium between nodal forces and internal forces is verified.

The sectional level deals with equilibrium within the cross-section at each integration point of the frame element. It relates the sectional or internal forces $\boldsymbol{s_s}$, with the generalized sectional deformations $\boldsymbol{e_s}$, see Eq. (1).

$$\begin{aligned} \boldsymbol{s_s} &= \{N\ V_y\ V_z\ T\ M_y\ M_z\}^T \\ \boldsymbol{e_s} &= \{\varepsilon_0\ \gamma_{0y}\ \gamma_{0z}\ \phi_x\ \phi_y\ \phi_z\}^T \end{aligned} \tag{1}$$

Where ε_0 is the axial elongation; γ_{0y} and γ_{0z} are the generalized shear deformations; and ϕ_x, ϕ_y and ϕ_z are the torsional and bending curvatures, respectively. A sectional stiffness matrix $\boldsymbol{k_s}$ is needed to perform the element state determination. $\boldsymbol{k_s}$ is a 6x6 matrix that, in general, is full, when full coupling of the six internal forces is accounted for.

The material level represents the description of the local response at a differential point. The variables are stress σ and strain ε tensors, and the material tangent matrix, $\boldsymbol{C}$. Depending on the constitutive model used, other internal variables are involved, such as plastic strains or damage variables. In a general 3D case, the concrete model needed to reproduce a general failure mode has to be triaxial.

In this paper, the problem of reproducing the response of a structure under general loading with different failure modes is tackled in a multilevel scheme, with 3 levels. At the element level, a force-based formulation that ensures the equilibrium between nodal and sectional forces is used. At the sectional level, a model that captures the coupling between the six internal forces while considering both longitudinal and transverse reinforcement is used. Finally, at the material level a 3D constitutive law for concrete is used to simulate the material behavior. In the following the models for the element, sectional and material levels are presented.

2.1. Beam-column formulation

The beam-column model developed in [7,9,22–24] and implemented in [27] is used at the element level. Assuming that there are no loads applied on the element, the force or flexibility approach consists on obtaining the force field as in Eq. (2).

$$\boldsymbol{s_s}(x) = \boldsymbol{b}(x)\boldsymbol{q} \tag{2}$$

Where $\boldsymbol{b}(x)$ contains the force interpolation functions that relates the nodal forces $\boldsymbol{q}$ with the internal forces on each cross-section $\boldsymbol{s_s}(x)$. The proper choice of the interpolation function leads to a strict satisfaction of equilibrium between nodal forces and section forces. The model requires the definition of a sectional constitutive relation that is written in an incremental way, as shown in Eq. (3).

$$\Delta\boldsymbol{e_s}(x) = \boldsymbol{f_s}(x)\Delta\boldsymbol{s_s}(x) = \boldsymbol{f_s}(x)\boldsymbol{b}(x)\Delta\boldsymbol{q} \tag{3}$$

where $\boldsymbol{f_s}(x) = \boldsymbol{k_s}^{-1}(x)$ is the sectional flexibility matrix. A compatibility condition between nodal displacement and sectional deformations can be written in a weak form, as in Eq. (4).

$$\boldsymbol{d} = \int_0^L \boldsymbol{b}^T(x)\boldsymbol{e_s}(x)dx \tag{4}$$

Following this approach, the element flexibility matrix that relates the nodal displacements with the nodal forces can be obtained as in Eq. (5).

$$\boldsymbol{F_e} = \int_0^L \boldsymbol{b}^T(x)\boldsymbol{f_s}(x)\boldsymbol{b}(x)dx \tag{5}$$

where $\boldsymbol{F_e} = \boldsymbol{K_e}^{-1}$.

Two different procedures for the element state determination were proposed by [7,9]. The proposed state determination in [7] iteratively computes the element forces and stiffness matrix while enforcing the element equilibrium and compatibility. In contrast, the algorithm proposed in [9] avoids the iterative procedure by introducing the residual nodal displacement in the force determination.

It can be seen in Eqs. (3)–(5) that the ability of reproducing any type of coupling between the internal forces relies directly on the sectional model. The cross-section discretization into uniaxial fibers is the most classical sectional model in the nonlinear analysis of reinforced concrete structures. This model robustly captures the axial-bending interaction while neglecting the coupling with tangential internal forces.

2.2. Sectional model

The cross-sectional model used in this framework is based on the displacement decomposition introduced in [28,29]. The displacement field that follows the plane section hypothesis $\boldsymbol{u_{ps}}$ is enhanced by means of a complementary displacement field that incorporates distortion and warping $\boldsymbol{u_w}$, see Eq. (6).

$$\boldsymbol{u} = \boldsymbol{u_{ps}} + \boldsymbol{u_w} = \begin{Bmatrix} u_{ps} \\ v_{ps} \\ w_{ps} \end{Bmatrix} + \begin{Bmatrix} u_w \\ v_w \\ w_w \end{Bmatrix} \tag{6}$$

The complementary field is determined by means of solving the three-dimensional equilibrium equations at the sectional level. The 3D stress and strain states are obtained on each material point of the cross section. As a result, the model is capable of reproducing the coupling of the six sectional internal forces for a general anisotropic material behavior as is the case of cracked concrete. This represents the main enhancement with respect to classic fiber section models.

The three-component complementary field is capable of reproducing the in-plane stretching of the cross section. Thus, the model includes explicitly the transverse reinforcements as stirrups or jackets. Considering the transverse reinforcements is crucial to reproduce shear or torsional failures. In addition, the interaction between stirrups or jackets with the surrounding concrete is the source of confinement. Therefore, confinement is reproduced naturally without the need of defining different constitutive law or material parameters on the same cross-section.

The numerical solution of the sectional equilibrium equations requires discretization of the complementary field. In [28,29] a FE model of the cross-section is used, see Eq. (7). In that FE context, $\boldsymbol{N_w}(y,z)$ represents the sectional interpolation matrix shape functions, and $\boldsymbol{d_w}$ is the vector of complementary nodal displacements. The terms in $\boldsymbol{d_w}$ are the main unknowns of the sectional problem. $\boldsymbol{d_w}$ is obtained by solving the three-dimensional equilibrium equations at the sectional level, as it is described in [25]. If nonlinear material behavior is considered, as is the case of concrete, the equilibrium problem is nonlinear.

$$\boldsymbol{u_w} = \boldsymbol{N_w}(y,z)\boldsymbol{d_w} \tag{7}$$

The sectional model is capable of reproducing in a consistent manner axial, shear, torsion and bending failures as well as coupled failures, as it was demonstrated in [28–30]. The main shortcoming of this model is its computational demand. The model was modified in [25] replacing the FE discretization by means of pre-defined functions on the cross-section domain, particularly in [25] b-splines functions were used. There, the interpolation matrix $\boldsymbol{N}_w(y,z)$ contains the b-splines shape functions, and the vector $\boldsymbol{d}_w$ are the weights factors of the b-spline interpolation and represent the additional internal degrees of freedom of the section. The hypothesis made in Eq. (7) is that the complementary field depends only on local information, thus the non-uniform warping and shear lag effects are neglected. Nevertheless, these effects are relevant in thin walled section rather than in compact cross sections as it is the case of most concrete beams or columns.

This numerical technique reduces significantly the number of degrees of freedom involved in the solution of the sectional problem, while the accuracy remains on the same level as in the original sectional model in [28–30]. Hence, the reduced computational demand of the b-spline sectional model makes it more suitable for the analysis of complete structures.

In this work the sectional model introduced in [25] is used as response model on the integration points of the frame formulation described before. The model proved to capture the sectional behavior in a consistent manner, with a reduced computational demand. Further details of the model can be found in [28–30,12,25].

2.3. Concrete constitutive model

Concrete is a complex material that exhibits several nonlinear phenomena. Within the same structure, there are different elements that may be under a wide range of loading conditions. Beams under high shear forces or columns with high levels of axial force and confinement are evidence of this. The sectional model presented in the previous section requires a 3D constitutive law. As the model aims to capture different failure modes, the constitutive equation has to be able to reproduce different stress conditions in a consistent manner.

The 3D plastic-damage model for concrete introduced in [31,32] and then implemented in [33] reproduces many of the main characteristic of concrete behavior. The main features of the plastic-damage model can be seen in Eqs. (8)–(12). The model is based on plasticity theory and introduces an isotropic stiffness degradation variable as it can be seen in Eq. (8). The stiffness degradation process and the elastoplastic evolution are decoupled to simplify the numerical computation as in [32]. The model follows the plasticity theory by defining the plastic strains ε^p as internal variable from which evolution is governed by the normality rule Eq. (9). The model is defined by two surfaces: the yield and plastic potential functions, Eq. (11) and Eq. (12), respectively.

$$\overline{\sigma} = \boldsymbol{E}_0 : (\varepsilon - \varepsilon^p) \;;\; \sigma = [1 - D(\kappa,\overline{\sigma})]\overline{\sigma} \tag{8}$$

$$\dot{\varepsilon^p} = \dot{\lambda}\frac{\partial \Phi}{\partial \overline{\sigma}}(\overline{\sigma}) \;;\; \dot{\kappa} = \dot{\lambda}\boldsymbol{H}(\overline{\sigma},\kappa) \tag{9}$$

$$\dot{\lambda} \geqslant 0;\; \dot{\lambda}F(\overline{\sigma},\kappa) = 0;\; F(\overline{\sigma},\kappa) \leqslant 0 \tag{10}$$

$$F(\overline{\sigma},\kappa) = \frac{1}{1-\alpha}\left[\alpha\overline{I_1} + \sqrt{3\overline{J_2}} + \beta(\kappa)\langle\widehat{\overline{\sigma}}_{max}\rangle - \gamma\langle -\widehat{\overline{\sigma}}_{max}\rangle\right] - c_c(\kappa) \leqslant 0 \tag{11}$$

$$\Phi(\overline{\sigma}) = \sqrt{\left(\varepsilon_1\alpha_p f_{t0}\right)^2 + 2\overline{J_2}} + \alpha_p\overline{I_1} \tag{12}$$

The model in [32] introduces two additional internal variables $\kappa = [\kappa_t, \kappa_c]$, one for tension and other compression, that play the role of hardening variables in a classic plasticity theory. Each one is defined as a measure of the dissipated energy during an uniaxial inelastic process, see Fig. 2. The evolution of the damage is governed by the exponential function for both tensile and compressive cases presented in Eq. (14)

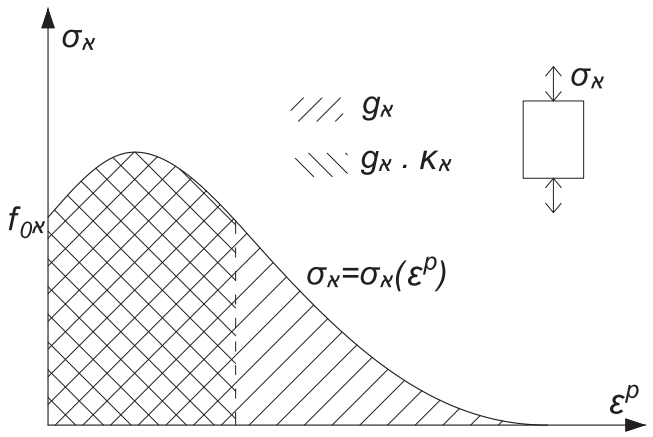

Fig. 2. Plastic-damage variable definition.

according to [32].

$$\kappa_{\aleph} = \frac{1}{g_{\aleph}}\int_0^{\varepsilon^p}\sigma_{\aleph}(\varepsilon^p)d\varepsilon^p \;\;;\;\; g_{\aleph} = \frac{G_{\aleph}}{l_{ch}} \tag{13}$$

$$\sigma_{\aleph}(\varepsilon_p) = f_{\aleph 0}\left[(1+a_{\aleph})exp(-b_{\aleph}\varepsilon_p) - a_{\aleph}exp(-2b_{\aleph}\varepsilon_p)\right] \tag{14}$$

In Eq. (13) the definition of the plastic-damage variables is presented. In a tensile case ($\aleph = t$), the dissipated energy is the fracture energy G_t; in a compressive case ($\aleph = c$), it is the so-called crushing energy G_c. Both are normalized by means of a localization length l_{ch} to ensure mesh objectivity, [34–36]. The definition of the characteristic length is defined in Section 2.4.

The evolution is governed by a non-associative flow rule that controls dilatancy by means of a single and constant parameter α_p in the plastic potential function Eq. (12). Dilatancy can be understood as the volume change of a granular material under shear strains. It affects the shear behavior of the material but also its transverse expansion. In [26], it was shown that a constant parameter fails to provide an objective description of the dilatant behavior. Hence, the original model needed specific calibration for different applications. To overcome this issue, a variable dilatancy parameter was introduced in [26]. In this paper, each concrete material point of each cross-section is simulated using the proposed model in [26]. The variable dilatancy parameter depends on the plastic-damage state κ and on the effective stress state $\overline{\sigma}$ as in Eq. (15).

$$\alpha_p = \alpha_p(\kappa,\overline{\sigma}) = \tan\psi(\kappa,\overline{\sigma}) \tag{15}$$

The dilatancy parameter is equal to zero for low levels of damage. Once dilatancy is activated it increases until it reaches its maximum value

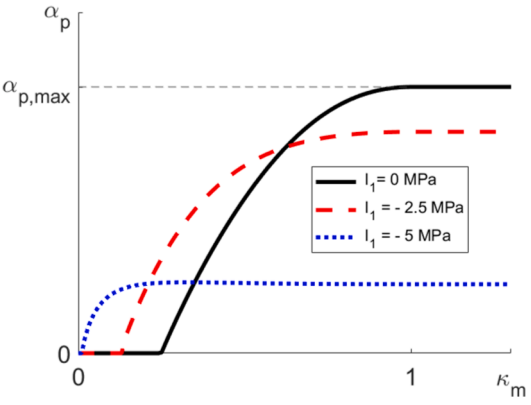

Fig. 3. Dilatancy evolution with damage and confining pressure.

$\alpha_{p,max}$, as it can be seen in Fig. (3). The presences of confinement reduces the effect of dilatancy. Thus, the maximum value $\alpha_{p,max}$ is made dependent on the confinement level through the first invariant of the stress tensor I_1, see Fig. (3).

The evolution of dilatancy is controlled by two material parameters: the maximum dilatancy ψ^{max} and internal friction ϕ^{max} angles. The evolutive dilatancy governs the shear softening and the nonlinear expansion of concrete without re-calibration of the material parameters. The constitutive model has shown in [26] that it is suitable for reproducing shear failure. Further, a study of confinement has been done in [25] showing that the model is able to capture confinement effects for different confining materials, geometries, and transverse reinforcement arrangements without needing re-calibration. Therefore, passive confinement can be traced in an objective manner. Further details on the constitutive model can be found in [26].

2.4. Implementation

The sectional and constitutive models are implemented on the object-oriented software OpenSees [27]. The plastic-damage model for concrete is implemented as a *NDMaterial* subclass of order six. The sectional model is implemented as a *SectionForceDeformation* subclass of order six. Both models can be used together with the *forceBeamColumn* element that corresponds to the frame formulation described in Section 2.1, see Fig. 4.

Thanks to the object-oriented structure of the software, different sectional models can be used within the same element. Furthermore, the sectional model presented in Section 2.2 is a local model which is independent of the behavior of the rest of the quadrature cross-sections. In addition, it only requires as an input the six-component vector of generalized strains. In this way, the b-spline cross-section model can be used where shear forces have a greater influence while on the rest of the sections a classic fiber discretization can be used. Thus, the computational resources can be optimized concentrating the effort on those region where the more complex behavior occurs. In addition, several integration methods are available for the frame element [23,37].

It is a well-known fact that force-beam elements tend to localize deformations when softening takes places [38,37]. This leads to a loss of objectivity and both the element and sectional responses depend on the number of integration points. To overcome this issue, in this work the energy regularization proposed by [38] is used. There, a constant energy release rate is proposed. In this work, the characteristic length l_{ch} used in the definition of the plastic-damage variables in Eq. (13) is made equal to the integration point length. This approach is followed in order to provide objectivity at the element level, but it is known that this leads to a loss of objectivity at the sectional level [23]. Extensive work has been made to solve this problem [39–44]. Most of these approaches involve non-local formulations and are based on particular frame formulations.

3. Validation

Three validation cases are presented to test the capabilities of the proposed framework. First, two beams belonging to the same experimental campaign carried out by [45] are numerically reproduced. Then, a reinforced concrete column cyclically loaded tested by [46] is simulated.

The following hypotheses are common to all cases: perfect bond is assumed between the reinforcements and the concrete mass. The longitudinal and transverse steel reinforcements are simulated using the *Giuffré-Menegotto-Pinto* uniaxial constitutive model with isotropic strain hardening [47]. The geometric nonlinearity is not consider in the simulation of beams and a linear geometric transformation is used in those cases. In the case of the simulation of the column, a P-Delta geometric transformation is used in order to take into account second-order effects.

The material parameters needed to define the concrete behavior are obtained from the reported data on the corresponding experimental campaigns. Those parameters not addressed by the test authors are estimated as proposed in [26].

3.1. Reinforced concrete beams

The response of two simply supported reinforced concrete beams tested by [45] is simulated with the proposed model. The selected specimens, named A1 and A3, were monotonically loaded by means of a single load applied in the mid-span. The geometry and reinforcement arrangements of the test can be seen in Fig. 5. Materials properties of the reinforcement and concrete are presented in Tables (1) and (2), respectively.

Taking into account the symmetry of the test, only half of the beams is modeled using a single element. The integration of the element response is made by means of three Gauss–Lobatto integration points. Additionally, a sensitivity analysis is made using 5 and 7 integration points to study the objectivity of the response for the two considered specimens.

The sectional model requires the definition of an interpolation grid to construct the b-spline interpolation functions. In both beams, 24 points are used to define the interpolation grid at the sectional domain, as it is shown in Fig. 6(a). The fiber distribution of both beams can be seen in Figs. 6(b) and (c). A total of 128 concrete material points are used on each cross-section; 32 fibers represent the transverse reinforcements; 7 and 9 fibers represent the longitudinal reinforcement in A1 and A3 specimens, receptively. A sensitivity analysis on the number of fibers and the number of b-spline functions was done in [25]. To simulate the test loading conditions, the mid-span vertical displacement is imposed in several steps.

The experimental response reported in [45] is compared against the

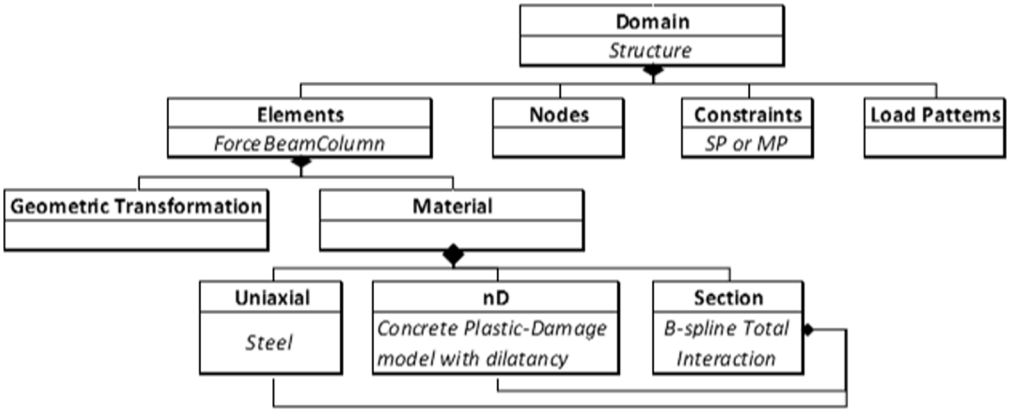

Fig. 4. Software structure.

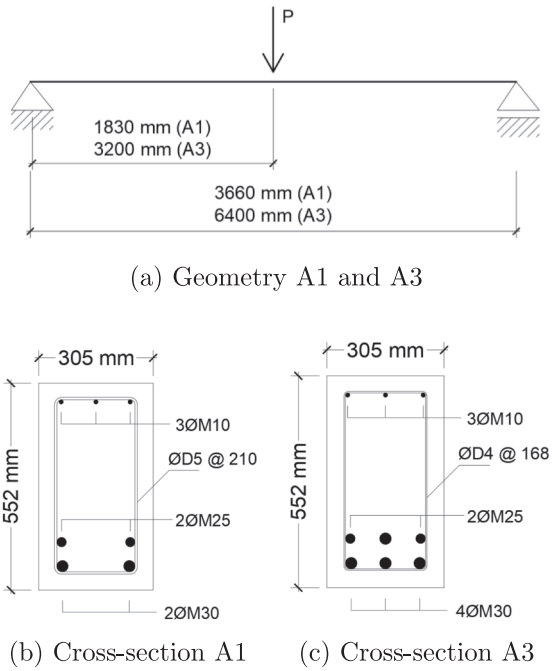

Fig. 5. Vecchio and Shim [45] test setup. Specimens A1 and A3.

Table 1
Reinforcement properties [45].

Bar Size	Diameter [mm]	f_y [MPa]	f_u [MPa]	E_s [MPa]
M10	11.3	315	460	200000
M25	25.2	445	680	220000
M30	29.9	436	700	200000
D4	3.7	600	651	200000
D5	6.4	600	649	200000

Table 2
Concrete properties [45].

Beam	f_c [MPa]	ε_0
A1	22.6	0.0016
A3	43.5	0.0019

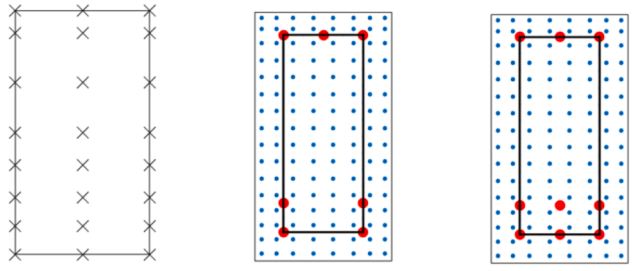

(a) Interpolation grid (b) Fiber distribution A1 (c) Fiber distribution A3

Fig. 6. Modeling details at the section domain of specimens A1 and A3.

load–deflection curves obtained with the proposed model for each specimen, see Figs. 7 and 9. In addition, two numerical responses obtained with beam models developed by other authors are presented. In [48], a plastic-damage model with constant dilatancy is properly condensed to be used in a mixed frame element. The 2D frame element in [13] uses a sectional model that takes into account the inter-fiber

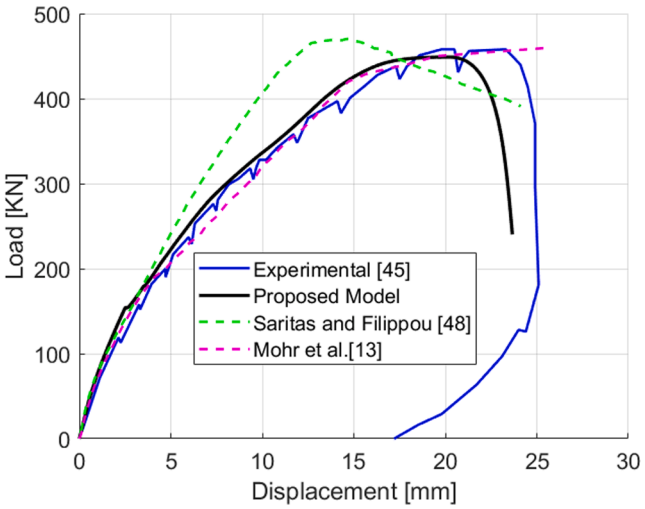

Fig. 7. Load–displacement curve for VS-A1 specimen. Experimental by [45].

equilibrium with a rotating smeared-crack constitutive model.

A very good agreement with the experimental response is obtained with the proposed model. Both the stiffness and ultimate load are well estimated. The softening branch on the response of specimen A1 is numerically captured even that a smaller ultimate displacement is predicted. In the case of A3, the analysis loses convergence after the initiation of the softening branch. Fig. 10 shows the objectivity of the response, it can be seen that refinement in the number of integration points does not change the results in a significant way.

The combined use of the plastic-damage model presented in [26] and with the sectional model in [25] results in an improvement with respect to the other frame elements. The element developed in [48] takes into account shear deformations in a simplified manner; then, it predicts a higher stiffness after cracking occurs. The presented model takes into account the complete interaction between shear and bending by means of the sectional model introduced in Section 2.2; therefore, it is able to capture the post-cracking stiffness in a more accurate way. The model in [13] also considers a sectional model with shear-bending interaction but uses a rotating smeared-crack constitutive model for concrete. It can be seen that it reproduces well the post-cracking behavior but it fails to capture the softening branch. The plastic-damage model described in Section 2.3, has demonstrated in [26] that, thanks to the variable dilatancy parameter, it is able to trace the material softening behavior in shear. Thus, the proposed model not only reproduces the interaction but also the shear softening behavior. The joint use of the constitutive, sectional and frame models exhibits the better agreement with the experimental results.

Notice that the two beams have identical cross-section dimensions while they differ on the span length and on the amount of reinforcements. On the experimental campaign, the shorter beam A1 exhibited a shear type failure while specimen A3 had a flexural type. It can be seen that the proposed model is able to capture both failure modes.

In Figs. 8 and 11 the state of a section located at $0.25L$ at the maximum load is presented. The different failure modes are reflected on the sectional state. The longitudinal stress distribution on both beams are different. In Figs. 8(a), specimen A1 shows a well defined region in the cracked part of the cross-section with compressive stresses, which can be interpreted as the projection of a compression strut intersecting the section. The stress distribution of specimen A3 in Figs. 11(a) is closer to a pure bending case, showing that in this case shear forces have a smaller influence. In addition, Figs. 8(c) and 11(c) show that on the vertical branches of the stirrups in beam A1 the yielding stress is reached while in the case of specimen A3 the stresses in the transverse reinforcement are on the elastic range ($f_y = 600\ MPa$).

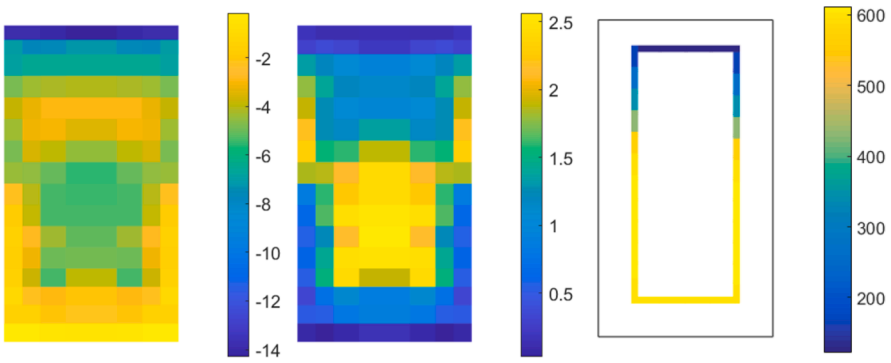

(a) σ_{xx} [MPa] (b) τ_{xz} [MPa] (c) σ_{st} [MPa]

Fig. 8. Sectional state A1. Section located at 0.25L. Maximum load.

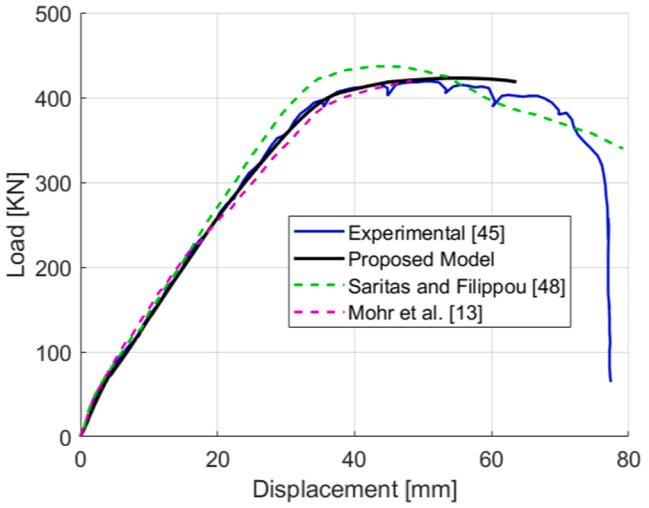

Fig. 9. Load–displacement curve for VS-A3 specimen. Experimental by [45].

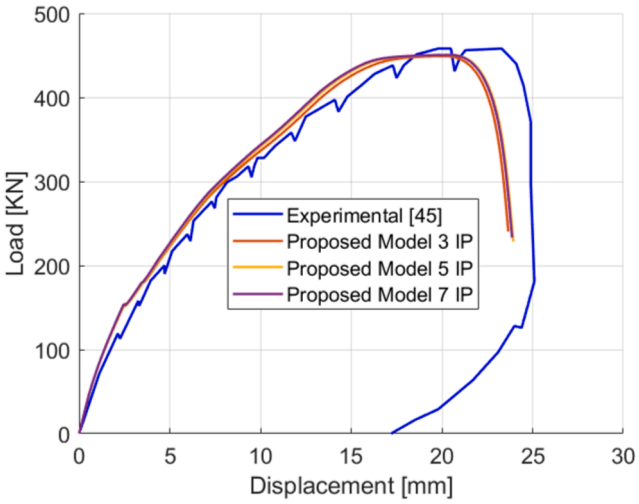

(a) VS-A1

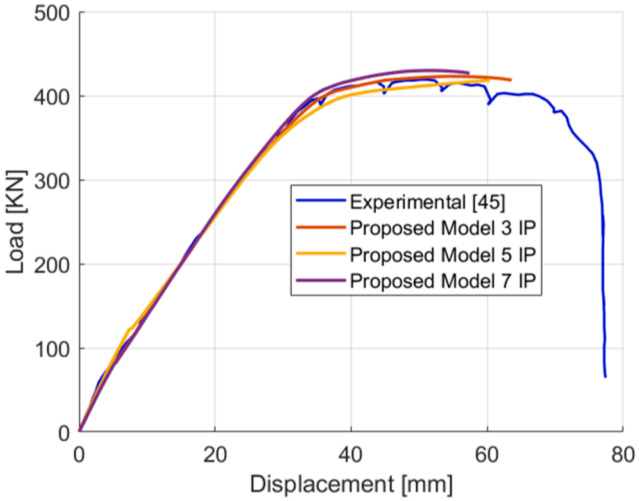

(b) VS-A3

Fig. 10. Sensitivity analysis. Experimental by [45].

3.2. Reinforced concrete column

The cyclic test of a reinforced concrete column in [46] is simulated with the proposed framework. Specimen 2CLH18 was first submitted to an axial load of $N = 503KN$ which remained constant during the rest of the test. Afterwards, the horizontal displacement at the top of the column was imposed in three cycles for different increments exceeding the yielding displacement. The geometry, reinforcement arrangements of the cross-section and boundary conditions are shown in Fig. 12. Concrete and steel material properties are presented in Table 3.

Thanks to the symmetry of the test, only one half of the column is modeled using a single element. The integration of the element response is made by means of six Gauss–Lobatto integration points. The interpolation grid in the cross-section domain consist of 4 points, corresponding with the corners of the cross-section, see Figs. 13(a). The fiber distribution that can be seen in Figs. 13(b) comprises 100 concrete fibers, 32 and 8 fibers for the transverse and longitudinal reinforcements, respectively.

Fig. 14 shows both the experimental and predicted load–displacement responses of the column. The overall behavior is suitably captured. The maximum strength of the column is well captured, as well as the ductility at the initiation of softening. The differences between experimental and simulated responses can be explained as follows. The tested column exhibited a strength loss on the last cycle due to the buckling of longitudinal bars. In addition, the experimental behavior shows more pinching, which is attributed to bond slip of the reinforcement. Neither the buckling of bars or the bond-slip effect are taken into account by the proposed model.

Fig. 15 presents the simulated moment, curvature and shear deformation distribution on the upper half of the column for three different levels of top displacement. It can be seen that curvatures tend to

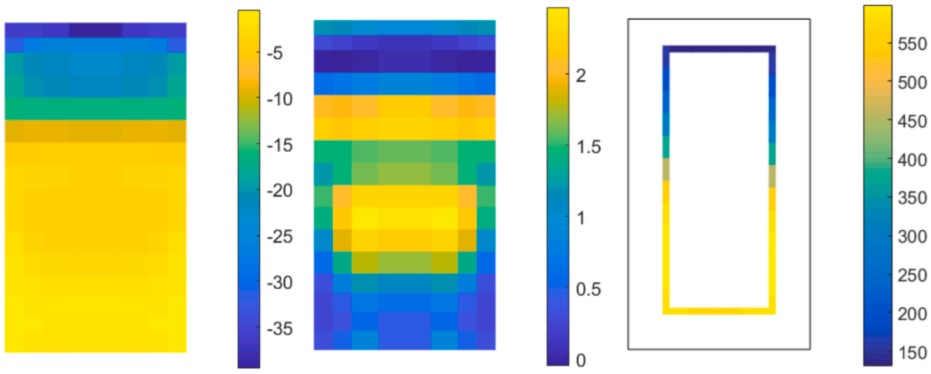

Fig. 11. Sectional state A3. Section located at 0.25L. Maximum load.

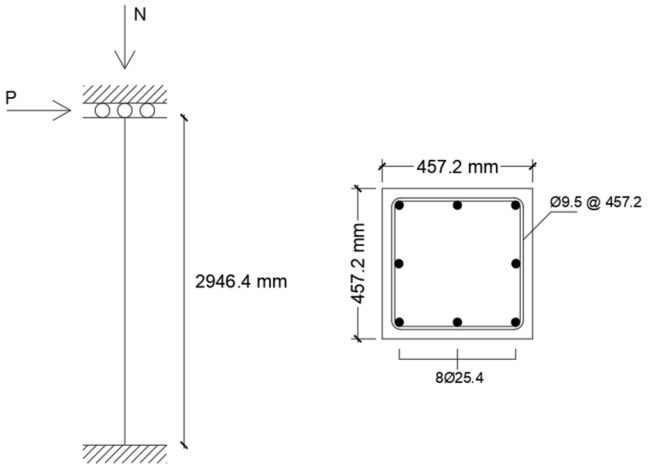

Fig. 12. Test setup specimen 2CLH18 [46].

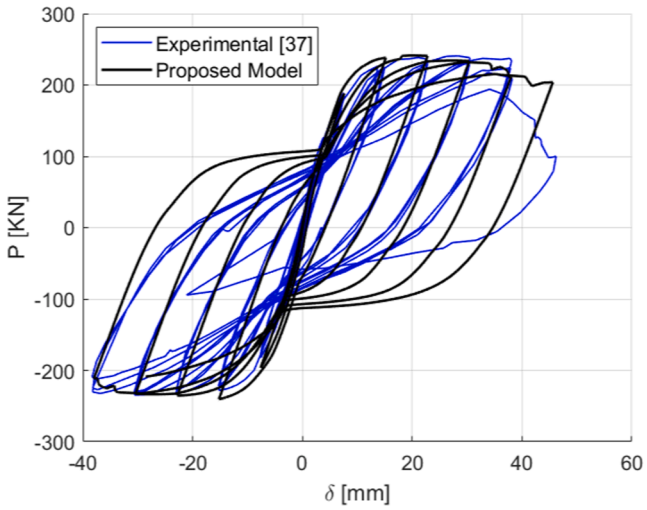

Fig. 14. Load–displacement curve for 2CLH18 specimen. Experimental by [46].

Table 3
Material properties [46].

Concrete			
f_c [MPa]	E_c [GPa]	ε_0	f_t [MPa]
33.1	28.77	0.002	2.2
Steel			
f_y long. [MPa]	f_y trans. [MPa]	E_s [GPa]	
331	400	200	

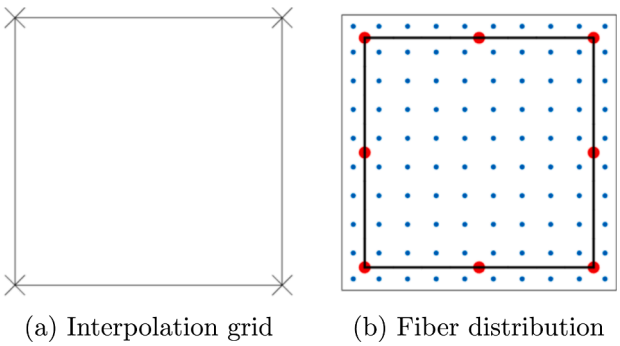

Fig. 13. Modeling details of specimen 2CLH18.

concentrate on the upper region which matches with the experimental observations reported in [46]. The maximum moment is almost identical on the displacements levels of $\delta = 15.20mm$ and $\delta = 30.30mm$ while on the last cycle $\delta = 45.25mm$ presents a strength loss of 11%.

The sectional state at the last level of top displacement can be seen in Fig. 16. Fig. 16(d) shows stresses on the longitudinal reinforcement, it is noticeable that the top and bottom bars have all reached the yielding stress. Stresses on the stirrups are presented in Fig. 16(c), the model does not predict yielding of the transverse reinforcement. Experimental observations report that yielding of the stirrups took place on the last cycle of the test. This difference can be explained by the fact that the transverse reinforcement is taken into account by means of a continuous steel line representing each tie, with tube of equivalent thickness is the ratio of the tie area and its spacing, while in the actual column stirrups are located at discrete positions. The measured strains on the experiment depend on how many discrete cracks have crossed the section and typically show greater variability than the numerical values. The latter are representative of the average stirrups strains in the region. Fig. 16(a-b) present the longitudinal and transverse stress distribution on the cross section which correspond to the stresses distributions of a flexural failure. Although the model can be improved by including other effects such as bond slip, the obtained response constitutes a good approximation and shows the capabilities of the model to handle dynamic loading conditions.

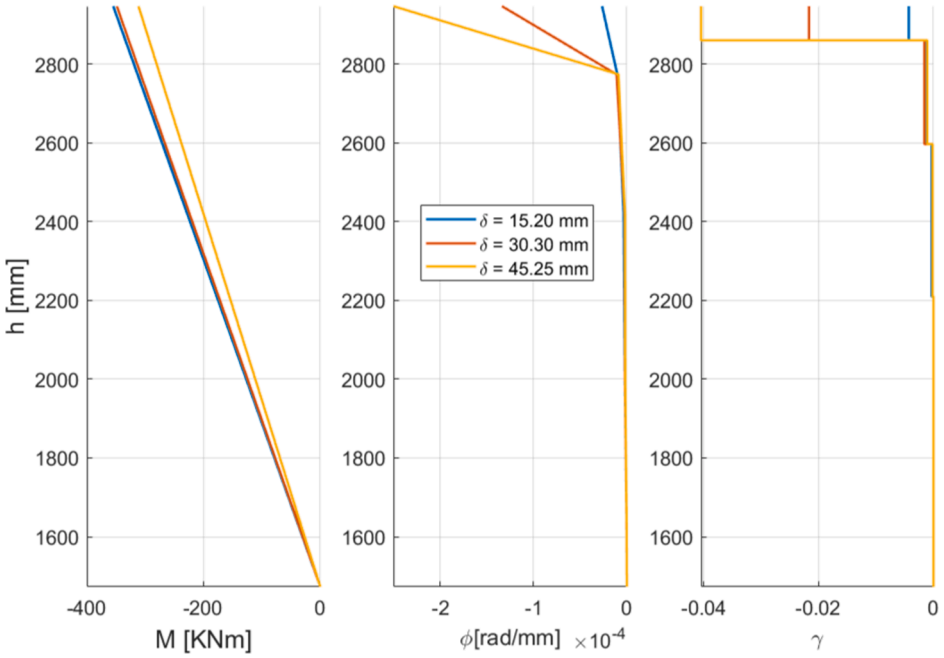

Fig. 15. Moment, curvature and shear deformations distributions on the upper part of the column.

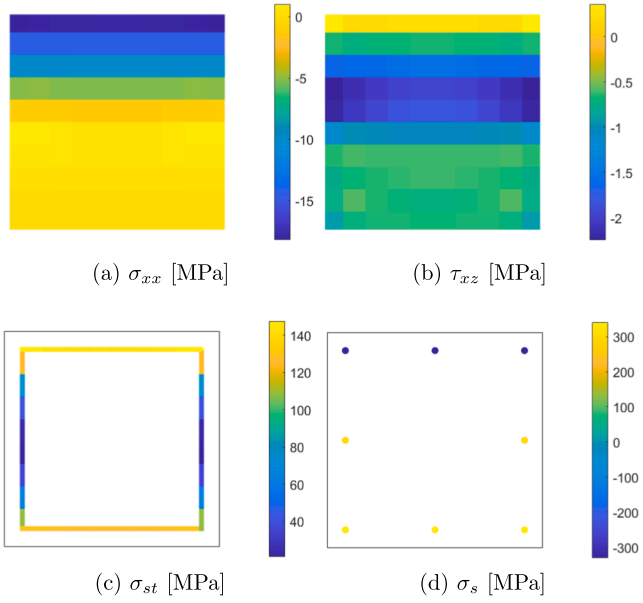

Fig. 16. Sectional state at $\delta = 45.25$ mm.

4. Application: Seismic performance of a road bridge

The seismic performance of a two-30 m-span bridge is analyzed using the proposed framework. Each span is formed by six simply-suported precast presstressed I girders; the bent comprises three circular columns of 1.20 m diameter and a cap beam; each end of the bridge has spill-through abutments to support the deck. See Fig. 17.

The bridge is simulated using only frame elements, the deck slab is replaced by a diaphragm constraint, see Fig. 18. The abutments are represented by zero-length elements that take into account elastomeric bearings stiffness, gaps, shear keys and the soil embankment behind the abutment, following the guidelines in [1]. The nonlinear behavior is expected to concentrate on the bent columns. Thus, girders and the cap beam are modeled using elastic elements. Furthermore, the connection between girders and the cap beam is made with two-node links taking into account the bearing flexibility, gaps, and shear keys. The mass of the deck is considered as additional distributed mass on the girder elements.

Each column is simulated by means of two force-based elements with four Gauss–Lobatto integration points. One b-spline section and 3 classic fiber models are used in each element. This is made in order to reduce the computational effort. The b-spline sections are located outside the D region of the element, where the shear failure may occur; this is at a minimum distance of a diameter form the elements end. The column reinforcement is defined in Fig. 18(b). Concrete strength is $f_c = 30$ *MPa* and steel yielding stress is $f_y = 420$ *MPa*. The cross-section is discretized into 508 concrete fibers, 70 transverse reinforcement fibers and 23 longitudinal reinforcement fibers, see Fig. 18(c). Five points are used to construct the b-spline interpolation functions as it is shown in Fig. 18(d).

The structure is subjected to the three component earthquake signal of the Chi-Chi 1999 event. The record is first scaled to match the maximum effective acceleration of 0.35*g*, which corresponds to the return period of 475 years at the site. Then, in order to study the bridge performance, the nonlinear time history analysis is made for six

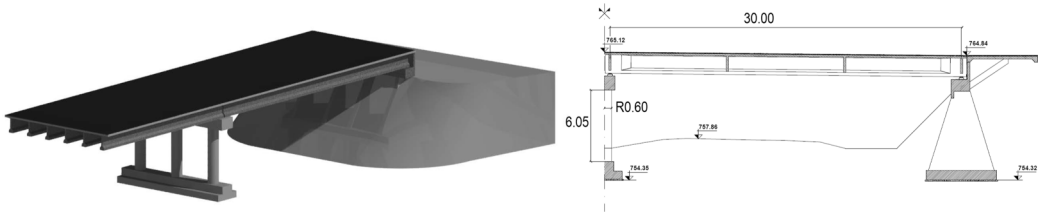

Fig. 17. Analyzed bridge.

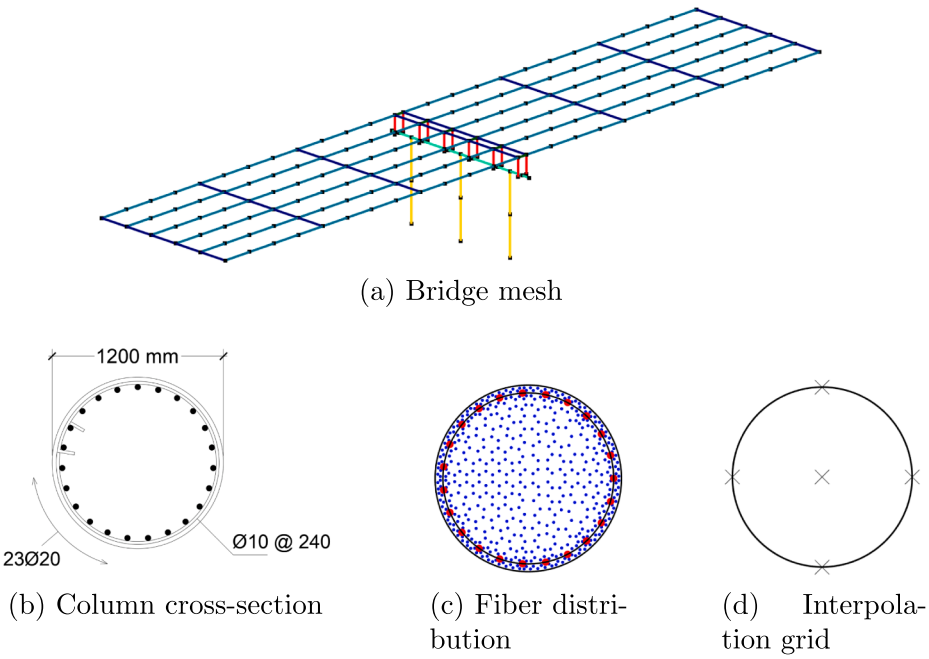

(a) Bridge mesh

(b) Column cross-section

(c) Fiber distribution

(d) Interpolation grid

Fig. 18. Bridge model.

intensities of the same earthquake representing different return periods ranging from 43 to 2475 years. Table 4 presents the different seismic intensities used in the analysis of the bridge.

Fig. 19 presents the maximum displacements in the longitudinal and transversal directions on the top of the central column for each one of the analyzed intensities. The analysis is also made with a classic fiber beam model in order to compare both simulations. It can be seen that both models predict a similar response on the longitudinal direction while, on the transverse one, the proposed model predicts bigger displacements. For instance, almost a 30% increment of the transverse displacement is obtained with the proposed model at the 0.35 g intensity. This is a consequence of considering additional deformations induced by shear damage in the column. The influence of shear deformations is greater on the higher intensities.

Fig. 20 presents the curvatures and shear deformations distribution on the central column height for the fifth intensity at the maximum displacement. It can be seen that curvatures tend to concentrate on the bottom sections for the longitudinal direction where the column acts as a cantilever column while on the transverse direction a double curvature profile is obtained. With regards to the shear deformations, they are only obtained on the b-spline sections, while on the classic fiber models they are not computed. Fig. (20) shows that the variable order framework allows considering different levels of complexity at different integration points, in this case shear deformation arises only from the b-spline sections and the rest of the sections have a zero contribution. The framework shows to be able to provide more information than classic models, such as shear deformations, concentration of damage, that improve decision taking in the design and assessment process.

Table 4
Seismic intensities.

Return Period	Annual	Intensity
[years]	Frequency	a_G [g]
43	0.02326	0.10
72	0.01389	0.14
108	0.00926	0.17
475	0.00211	0.35
1033	0.00097	0.48
2475	0.00040	0.64

5. Conclusions

A new framework for the analysis of frame structures under general loading is proposed. The framework is based on three levels: element, sectional and concrete constitutive levels. The combined use of the presented models enables the numerical reproduction of different failures modes such as flexural, shear, torsion or axial, as well as coupled modes. Furthermore, as it explicitly considers the transverse reinforcement, it can naturally reproduce the effect of confinement and the steel contribution on the shear strength.

Although the frame model and sectional models can be used with any 3D constitutive model, the use of a proper material model shows to be crucial for reproducing different failures modes in a consistent way.

Validation shows that the model reproduces well the experimental data for beams and columns under monotonic and cyclic loads. A sensitivity analysis was made considering different number of integration points along a shear failing specimen. It was shown that the overall response and the estimated ductility does not show significant influence on the number of integration points. The observed maximum variation in the estimated deformability was 10%. Therefore, it may be stated that the implemented regularization strategy allows for an effective control of localization issues.

Cyclic loading on columns non-conforming current code detailing, such as the one in Fig. (14), was adequately captured in terms of shear capacity and lateral deformation, although the model predicted less degradation and pinching. This difference was attributed to bond-slip and its degradation during cyclic loading, which were not considered in the simulation.

The same framework can be used in all the elements of a complete structure. Furthermore, as the element allows the use of different sectional models on the integration points, the framework gives the user the flexibility to use the more refined sectional model only where coupling between the internal forces is more important or where local sectional information is needed.

The study of a bridge performance shows that the model is robust and that is able to analyze full-scale structures. The model can be used to make performance assessments including all the possible failures modes. This, cannot be done with classic fiber-beam models showing the major improvement of the presented framework. Although the bridge structure

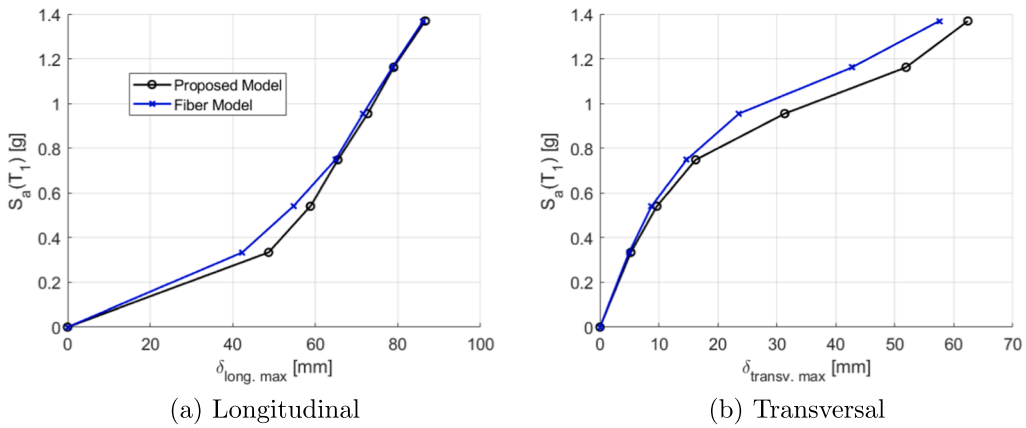

(a) Longitudinal (b) Transversal

Fig. 19. Incremental dynamic analysis response.

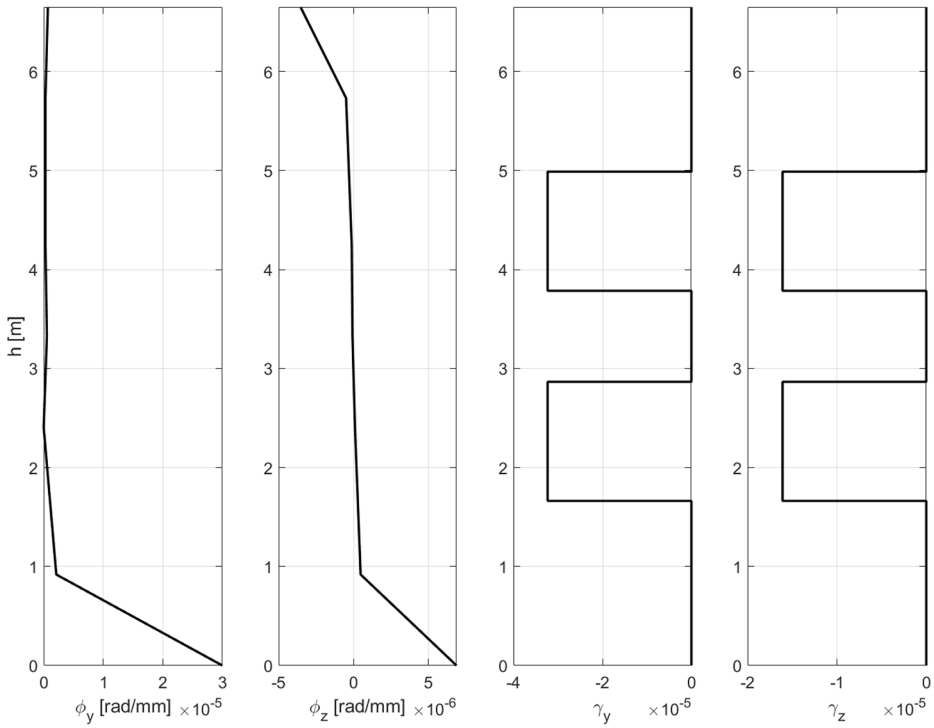

Fig. 20. Central column deformations at maximum displacement.

was designed following current code provisions, the results show an increment of up to 36% of the lateral deformability when considering the effects of lateral forces and torsion through the current framework, compared to traditional fibre discretization. Therefore, adequate consideration of transversal effects may significantly affect the assessment of seismic damage.

Declaration of Competing Interest

The authors declare that they have no known competing financial interests or personal relationships that could have appeared to influence the work reported in this paper.

Acknowledgments

The first and second authors acknowledge the support provided by Spanish Ministry of Economy, Industry and Competitiveness and the European Regional Development Fund (ERDF), through the projects BIA2015-64672-C4-1R, BIA2012-36848 and RTI2018-097314-B-C21. The first author acknowledges the support of the Catalan Agency for University and Research through doctoral scholarship 2018FI-B1-00103. The third author acknowledges the support of the Research Council of Universidad Nacional de Rosario (CIUNR) and the Science and Technology Secretariat (SECyT), through the project 1ING601.

References

[1] CALTRANS, Seismic Design Criteria Ver.2.0, State of California Deparment of Transportation, Sacramento, CA, 2019.
[2] FEMA, P-58: Seismic Performance Assessment of Buildings, Federal Emergency Management Agency, Washington,DC, 2018.
[3] ACI Committee 341, ACI 341.3R07: Seismic Evaluation and Retrofit Techniques for Concrete Bridges, American Concrete Institute, Farmington Hills, 2007.
[4] AASHTO. Guide Specification for LRFD Seismic Bridge Design. 2nd Edition,. Washington, DC: American Association of State Highway and Transportation Officials; 2011.
[5] Carol I, Murcia J. Nonlinear time-dependent analysis of planar frames using an 'exact' formulation–i. theory. Computers & Structures 1989;33:79–87.

[6] F. Taucer, E. Spacone, F. Filippou, A fiber beam-column element for seismic response analysis of reinforced concrete structures, Technical Report 17, Earthquake Engineering Research Center, 1991.
[7] Spacone E, Ciampi V, Filippou F. Mixed formulation of nonlinear beam finite element. Computers & Structures 1996;58:71–83.
[8] Spacone E, Filippou FC, Taucer FF. Fibre beam column model for non-linear analysis of R/C frames: Part I. formulation. Earthquake Engineering & Structural Dynamics 1996;25:711–25.
[9] Neuenhofer A, Filippou FC. Evaluation of nonlinear frame finite-element models. Journal of Structural Engineering 1997;123:958–66.
[10] Ranzo G, Petrangeli M. A fibre finite beam element with section shear modelling for seismic analysis of RC structures. J. Earthquake Eng. 1998;2:443–73.
[11] Ceresa P, Petrini L, Pinho R. Flexure-shear fiber beam-column elements for modeling frame structures under seismic loading – state of the art. J. Earthquake Eng. 2007;11:46–88.
[12] Bairán JM, Marí AR. Shear-bending-torsion interaction in structural concrete members: A nonlinear coupled sectional approach. Archives of Computational Methods in Engineering 2007;14:249–78.
[13] Mohr S, Bairán JM, Marí AR. A frame element model for the analysis of reinforced concrete structures under shear and bending. Eng. Struct. 2010;32:3936–54.
[14] Le Corvec V. Nonlinear 3D frame element with multi-axial coupling under consideration of local effects. Ph.D. thesis. Berkeley: Department Civil and Environmental Engineering, University of California; 2012.
[15] Li Z-X, Gao Y, Zhao Q. A 3D flexure–shear fiber element for modeling the seismic behavior of reinforced concrete columns. Eng. Struct. 2016;117:372–83.
[16] Kagermanov A, Ceresa P. Fiber-section model with an exact shear strain profile for two-dimensional rc frame structures. Journal of Structural Engineering 2017;143:04017132.
[17] Kolozvari K, Orakcal K, Wallace JW. New opensees models for simulating nonlinear flexural and coupled shear-flexural behavior of RC walls and columns. Computers & Structures 2018;196:246–62.
[18] Re PD, Addessi D, Filippou FC. Mixed 3D beam element with damage plasticity for the analysis of RC members under warping torsion. Journal of Structural Engineering 2018;144:04018064.
[19] Kagermanov A, Ceresa P. 3D fiber-based frame element with multiaxial stress interaction for RC structures. Advances in Civil Engineering 2018;2018.
[20] Rajapakse R, Wijesundara K, Nascimbene R, Bandara C, Dissanayake R. Accounting axial-moment-shear interaction for force-based fiber modeling of RC frames. Eng. Struct. 2019;184:15–36.
[21] Nguyen T-A, Nguyen Q-H, Somja H. An enhanced finite element model for reinforced concrete members under torsion with consistent material parameters. Finite Elem. Anal. Des. 2019;167:103323.
[22] Scott MH, Franchin P, Fenves GL, Filippou FC. Response sensitivity for nonlinear beam-column elements. Journal of Structural Engineering 2004;130:1281–8.
[23] Scott MH, Fenves GL. Plastic hinge integration methods for force-based beam-column elements. Journal of Structural Engineering 2006;132:244–52.
[24] Scott MH, Fenves GL, McKenna F, Filippou FC. Software patterns for nonlinear beam-column models. Journal of Structural Engineering 2008;134:562–71.
[25] Poliotti M, Bairán J-M. B-spline sectional model for general 3D effects in reinforced concrete elements. Eng. Struct. 2020;207:110200.
[26] Poliotti M, Bairán J-M. A new concrete plastic-damage model with an evolutive dilatancy parameter. Eng. Struct. 2019;189:541–9.
[27] McKenna F, Scott MH, Fenves GL. Nonlinear finite-element analysis software architecture using object composition. Journal of Computing in Civil Engineering 2010;24:95–107.
[28] Bairán JM, Marí AR. Coupled model for the non-linear analysis of anisotropic sections subjected to general 3D loading. Part 1: Theoretical formulation. Computers & Structures 2006;84:2254–63.
[29] Bairán JM, Marí AR. Coupled model for the nonlinear analysis of sections made of anisotropic materials, subjected to general 3D loading. Part 2: Implementation and validation. Computers & Structures 2006;84:2264–76.
[30] Bairán JM, Marí AR. Multiaxial-coupled analysis of RC cross-sections subjected to combined forces. Eng. Struct. 2007;29:1722–38.
[31] Lubliner J, Oliver J, Oller S, Oñate E. A plastic-damage model for concrete. Int. J. Solids Struct. 1989;25:299–326.
[32] Lee J, Fenves GL. Plastic-damage model for cyclic loading of concrete structures. Journal of Engineering Mechanics 1998;124:892–900.
[33] ABAQUS. Theory manual version 6.12. Abaqus Documentation; 2012.
[34] Bazant Z. Instability, ductility, and size effect in strain-softening concrete. Journal of Engineering Mechanics - ASCE 1976;102:331–44.
[35] Bazant Z. Comment on orthotropic models for concrete and geomaterials. Journal of Engineering Mechanics - ASCE 1983;109:849–65.
[36] Oliver J. A consistent characteristic length for smeared cracking models. Int. J. Numer. Meth. Eng. 1989;28:461–74.
[37] Scott MH, Hamutçuoglu OM. Numerically consistent regularization of force-based frame elements. Int. J. Numer. Meth. Eng. 2008;76:1612–31.
[38] Coleman J, Spacone E. Localization issues in force-based frame elements. Journal of Structural Engineering 2001;127:1257–65.
[39] Addessi D, Ciampi V. A regularized force-based beam element with a damage–plastic section constitutive law. Int. J. Numer. Meth. Eng. 2007;70:610–29.
[40] Kenawy M, Kunnath S, Kolwankar S, Kanvinde A. Concrete uniaxial nonlocal damage-plasticity model for simulating post-peak response of reinforced concrete beam-columns under cyclic loading. Journal of Structural Engineering 2020;146:04020052.
[41] Kenawy M, Kunnath S, Kolwankar S, Kanvinde A. Fiber-based nonlocal formulation for simulating softening in reinforced concrete beam-columns. Journal of Structural Engineering 2018;144:04018217.
[42] Feng D, Ren X, Li J. Implicit gradient delocalization method for force-based frame element. Journal of Structural Engineering 2016;142:04015122.
[43] Valipour HR, Foster SJ. Nonlocal damage formulation for a flexibility-based frame element. Journal of Structural Engineering 2009;135:1213–21.
[44] Zhang G, Khandelwal K. Modeling of nonlocal damage-plasticity in beams using isogeometric analysis. Computers & Structures 2016;165:76–95.
[45] Vecchio FJ, Shim W. Experimental and analytical reexamination of classic concrete beam tests. Journal of Structural Engineering 2004;130:460–9.
[46] Lynn AC, Moehle JP, Mahin SA, Holmes WT. Seismic evaluation of existing reinforced concrete building columns. Earthquake Spectra 1996;12:715–39.
[47] F.C. Filippou, V.V. Bertero, E.P. Popov, Effects of bond deterioration on hysteretic behavior of reinforced concrete joints, Report EERC 83-19, Earthquake Engineering Research Center, University of California Berkeley, 1983.
[48] Saritas A, Filippou FC. Numerical integration of a class of 3d plastic-damage concrete models and condensation of 3d stress–strain relations for use in beam finite elements. Eng. Struct. 2009;31:2327–36.